Solar Energy Materials & Solar Cells 155 (2016) 30–37

Contents lists available at ScienceDirect

Solar Energy Materials & Solar Cells

journal homepage: www.elsevier.com/locate/solmat

Small molecules based on tetrazine unit for efficient performance solution-processed organic solar cells

Pengfei Ma [a], Chen Wang [a], Shanpeng Wen [a,*], Lu Wang [a], Liang Shen [a], Wenbin Guo [a], Shengping Ruan [a,b,**]

[a] State Key Laboratory on Integrated Optoelectronics and College of Electronic Science & Engineering, Jilin University, Changchun 130012, PR China
[b] State Key Laboratory on Applied Optics, Changchun 130012, PR China

ARTICLE INFO

Article history:
Received 8 March 2016
Received in revised form
29 April 2016
Accepted 2 May 2016
Available online 13 May 2016

Keywords:
Tetrazine unit
Small molecules
Low HOMO level
Organic solar cell

ABSTRACT

Two D2-A-D1-A-D2 type small molecules using Benzo[1,2-b:4,5-b′]dithiophene (BDT) as central building block, tetrazine (Tz) as an electron accepting moiety, bithiophene or terthiophene as end donor units were synthesized. The optical and electrochemical properties of synthesized molecules indicate that these molecules can absorb sunlight in a broad spectral range from 300 to 700 nm and show suitable energy level for efficient exciton dissociation. The introduction of tetrazine unit in these molecules effectively reduces the highest occupied molecular orbital (HOMO) energy levels of these molecules, thus increases air stability of these molecules as well as the open circuit voltage (V_{oc}) in photovoltaic devices. Bulk heterojunction organic solar cells were fabricated by blending of these molecules with [6,6]-phenyl-C_{71}-butyric acid methyl ester ($PC_{71}BM$) on indium tin oxide/glass substrates. This work afford promising power conversion efficiencies over 5.0%, with a large V_{oc} of 0.98 V, measured under air mass 1.5 global irradiation of 100 mW/cm^2.

1. Introduction

Organic solar cells (OSCs) have attracted much attention because of the potential as a competitive technology of green energy with the advantages of solution processability, low cost, light weight and high mechanical flexibility [1–4]. Over the past decades, polymer based OSCs with bulk heterojunction (BHJ) architecture made great progress in achieving high power conversion efficiencies (PCEs) [5–8]. Recently, PCE has increased remarkably and approached greater than 10% based on polymer donors and fullerene derivative acceptors [9–11]. However, it cannot be denied that there are disadvantages for polymer based OSCs, such as undefined molecule weight, polydispersity, low purity, and batch-to-batch variations. In contrast, small molecule (SM) donors have been intensively researched as competitive alternative to their polymer counterparts due to their advantages of monodispersity, simple synthesis, high purity, greater solubility, good reproducibility and easier band structure control [12–15]. Up to now SMs have shown a great potential for solar cell application, with the highest PCEs over 9% [16–19]. However further advancement towards commercialization still requires the design and synthesis of new SMs.

One feasible approach for obtaining organic conjugated molecule is to design donor-acceptor (D-A) architecture with alternating electron donor and electron acceptor moiety among the organic molecular backbone. The D-A type organic molecules can not only narrow band gap by utilizing intramolecular charge transfer transition between electron donor unit and acceptor unit inside molecules, but also adjust the HOMO and LUMO energy levels through selecting different donor or acceptor moiety into the molecular backbone [20–22]. The HOMO energy level of organic molecules is an important parameter for designing donor material of OSCs because the V_{oc} of BHJ OSCs is determined by the difference between of the LUMO level of PCBM and the HOMO level of organic molecule [23–25].

Tetrazine (Tz) has been a promising building block as a electron acceptor unit in D-A conjugated polymers, because relatively strong electron withdrawing ability of Tz would help to lower HOMO and LUMO energy levels of corresponding conjugated polymers, which is conductive to improving V_{oc} in BHJ OSCs [26–29]. For instance, it has been reported that a narrow bad gap copolymer, PCPDTTBTT, composed of cyclopenta[2,1-*b*:3,4-*b*′] dithiophene (CPDT) and benzothiadiazole (BT) as the D and A units, respectively, shows HOMO and LUMO energy levels of −5.12 and −3.39 eV, respectively [27]. When the BT unit in PCPDTTBTT is replaced by Tz unit, the copolymer (PCPDTTTz) exhibits lower

* Corresponding author.
** Corresponding author at: State Key Laboratory on Integrated Optoelectronics and College of Electronic Science & Engineering, Jilin University, Changchun 130012, PR China.
E-mail address: sp_wen@jlu.edu.cn (S. Wen).

http://dx.doi.org/10.1016/j.solmat.2016.05.003
0927-0248/

HOMO and LUMO energy levels of −5.35 and −3.52 eV, respectively [28]. Another copolymer (PBDT-TTz) composed of Benzo[1,2-b:4,5-b′]dithiophene (BDT) as D unit and Tz as A unit also exhibits relatively low HOMO and LUMO energy levels of −5.42 and −3.58 eV [29]. It suggests that the introduction of Tz moiety in D-A polymer backbone effectively reduce the HOMO energy levels of the copolymers and thus enhance the V_{oc} of photovoltaic device. In addition, the band gap of corresponding copolymer has not suffered from obvious increase after incorporating Tz unit [30]. This suggests us to design new Tz-based SMs to achieve high V_{oc} without significant losses in J_{sc}.

On the other hand, BDT is one of the most commonly employed electron donating building block of conjugated polymer materials for organic optoelectronic applications, especially for OSCs devices [31–33]. Because its relatively large and planar conjugated structure greatly enhance facial π-π stacking of the molecules, thus it benefit charge transportation and red shift of the absorption spectra of these conjugated polymers. The unique properties of BDT structure leads to the BDT-based polymer possess the advantage of not only high hole mobility in field effect transistor (FET) but also high PCE in OSCs. Therefore, the BDT is a promising electron donating unit in designing novel organic molecules for high performance photovoltaic cells.

In this paper, we designed and synthesized two new organic molecules with a D2-A-D1-A-D2 architecture, where D1 is BDT structure as a center and electron donating unit, thiophene or bithiophene as π-bridge, A is Tz as an electron withdrawing unit, and D2 is bithiophene or terthiophene as a electron donating unit and π-conjugation extender. We investigated the effects of π-bridge length and end groups on absorption, energy level and photovoltaic properties of these molecules. The photovoltaic devices fabricated from the two SMs with a structure of ITO/PEDOT/SM:$PC_{71}BM$/LiF/Al afforded PCEs of 5.01% and 5.29% under one sun of AM 1.5 solar simulator illumination (100 mW/cm^2). It is worthwhile to mention that the high V_{oc}s of 0.88 and 0.98 V derived from these devices due to the deep HOMO energy levels of these two molecules.

2. Results and discussion

2.1. Synthesis and characterization

The synthesis routes of these two D2-A-D1-A-D2 type SMs are presented in Scheme 1. Compounds 1 [27] and 3 [31] were synthesized according to the references. The new intermediate compound 2 and 6 were synthesized via stille coupling reaction between compound 1 or compound 5 and trimethyl(5-hexylthiophene-2-yl)stannane [34,35] using $Pd(PPh_3)_4$ as catalyst. Bromination of 4 with *N*-bromosuccinimide afforded compound 5 in a mixture of chloroform and acetic acid with a yield of 88%. At last, compound 3 was reacted with compounds 2 and 6 to obtain the two SMs $BDT(TTzT)_2$ and $BDT(TTz2T)_2$ though Stille coupling reaction. These synthesized molecules exhibited good solubility in common organic solvents such as dichloromethane, chloroform, and chlorobenzene at room temperature, which provides the solution-processed thin films for photovoltaic applications Fig. 1.

2.2. Optical properties

The UV–vis absorption spectra of the synthesized molecules in dilute chloroform solution and in sold films are shown in Fig. 2, and the main optical properties are summarized in Table 1. Both molecules exhibited a relatively broad absorption range covering the wavelength from 300 to 600 nm in solution. The maximum absorption (λ_{max}^{sol}) of $BDT(TTz2T)_2$ was 489 nm, which was red-shifted by 10 nm compared with that of $BDT(TTzT)_2$, because the extending π-bridge and end group in $BDT(TTz2T)_2$ backbone lead to extending molecular conjugated length. The molar absorption coefficients of $BDT(TTz2T)_2$ solution is $1.27 \times 10^5\ M^{-1}\ cm^{-1}$ at the maximum absorption wavelength, quite larger than $7.29 \times 10^4\ M^{-1}\ cm^{-1}$ of $BDT(TTzT)_2$ solution. Fig. 2(b) shows optical absorption spectra of thin film of these molecules. The absorption spectra of thin films exhibit broader response range than that in solution. The maximum absorption peaks of thin films are red-shifted 49 and 43 nm respectively compared with that in solution, and thus indicating a strong intermolecular π-π interaction in solid state [36]. The absorption coefficients of thin film of

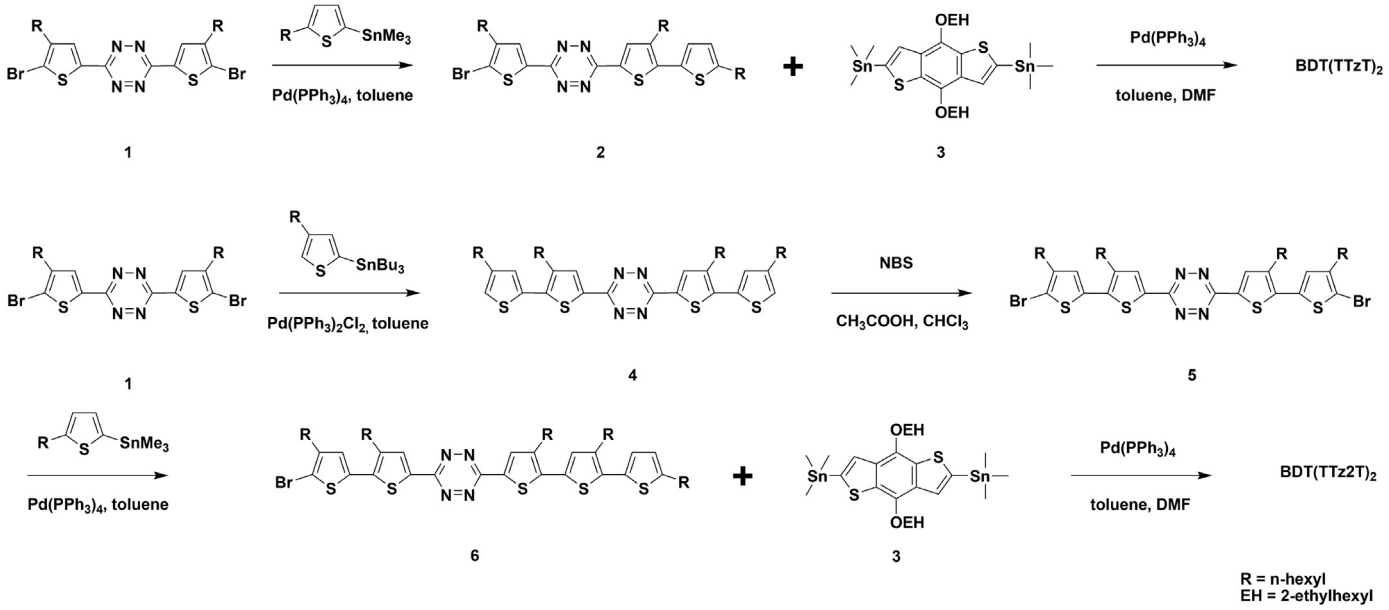

Scheme 1. Synthetic routes of $BDT(TTzT)_2$ and $BDT(TTz2T)_2$.

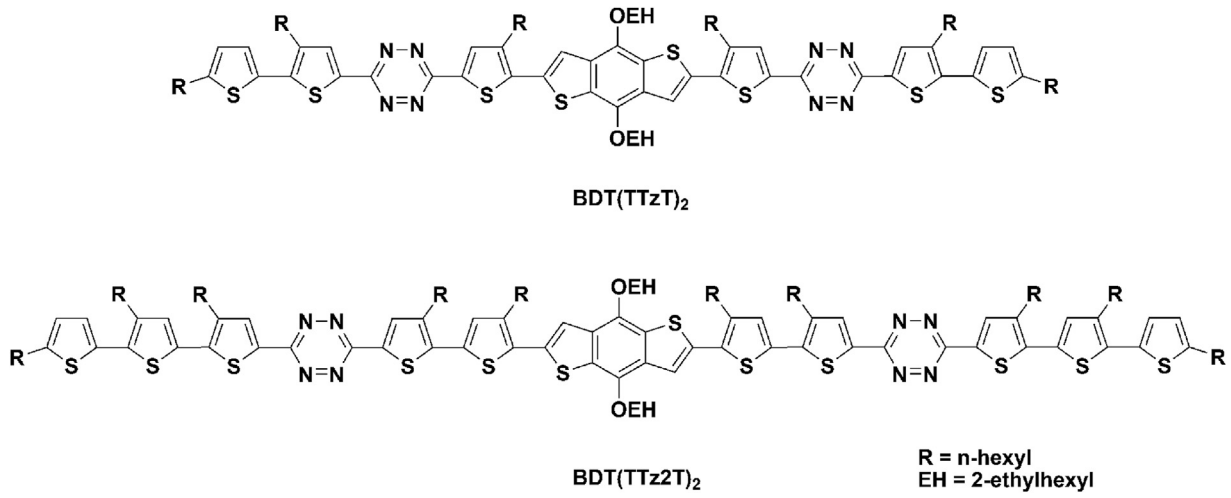

Fig. 1. Chemical structures of $BDT(TTzT)_2$ and $BDT(TTz2T)_2$.

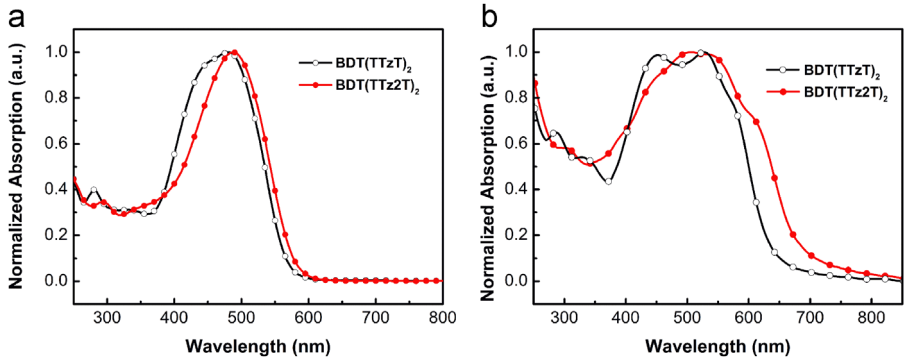

Fig. 2. UV–vis absorption spectra of $BDT(TTzT)_2$ and $BDT(TTz2T)_2$ (a) in chloroform solution and (b) in solid films.

Table 1
Optical and electrochemical data of $BDT(TTzT)_2$ and $BDT(TTz2T)_2$.

	λ_{max}^{sol} (nm)	ε^{sol} (M^{-1} cm^{-1})	λ_{max}^{film} (nm)	ε^{film} (cm^{-1})	E_g^{opt} (eV)	E_{ox}^{onset} (V)	HOMO (eV)	E_{red}^{onset} (V)	LUMO (eV)	E_g^{ec} (eV)
$BDT(TTzT)_2$	479	7.29×10^4	452/528	3.49×10^4	1.91	0.97	−5.51	−0.87	−3.67	1.84
$BDT(TTz2T)_2$	489	1.27×10^5	508/532	4.09×10^4	1.77	0.76	−5.30	−0.90	−3.64	1.66

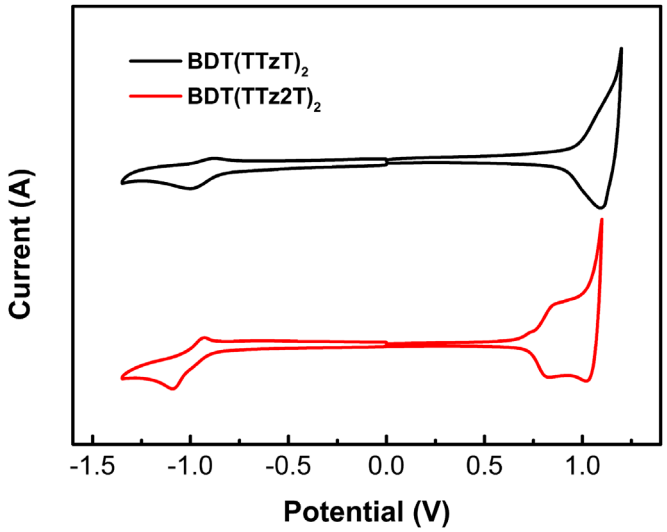

Fig. 3. Cyclic voltammograms curves of $BDT(TTzT)_2$ and $BDT(TTz2T)_2$ film on platinum electrode in 0.1 mol/L n-Bu4NPF6 in CH3CN solution.

$BDT(TTzT)_2$ and $BDT(TTz2T)_2$ show the same trend with those in solution, which are listed in Table 1. The optical band gaps (E_g^{opt}) of $BDT(TTzT)_2$ and $BDT(TTz2T)_2$ calculated from the absorption edges in the solid state are 1.91 and 1.77 eV, respectively.

2.3. Electrochemistry properties

Cyclic voltammetry is carried out to investigate the redox behavior of SMs and to estimate their LUMO and HOMO energy levels. The measurements of SMs in films were performed in acetonitrile with 0.1 M tetrabutylammonium hexafluorophosphate ($TBAPF_6$) as the supporting electrolyte, with platinum button working electrodes, a platinum wire counter electrode, and an $Ag/AgNO_3$ reference electrode under a N_2 atmosphere. Ferrocene/ferrocenium was used as the internal standard.

Fig. 3 showed the redox curves of the SMs. On the anodic test, the SMs exhibited a reversible oxidation with onset potentials of 0.97 V (versus Ag/Ag^+) for $BDT(TTzT)_2$ and 0.76 V for $BDT(TTz2T)_2$, respectively. In contrast, the cathodic test exhibited onset reduction potentials of −0.87 V for $BDT(TTzT)_2$ and −0.90 V for $BDT(TTz2T)_2$. The HOMO and LUMO energy levels as well as electrochemical

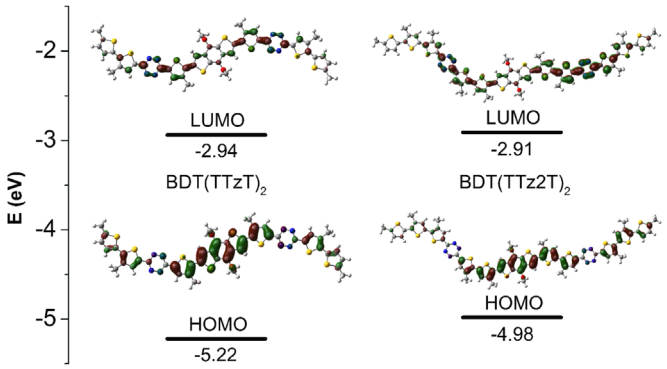

Fig. 4. DFT-calculated LUMO and HOMO of the geometry optimized structures of $BDT(TTzT)_2$ and $BDT(TTz2T)_2$.

Table 2
Summary of device parameters of OSCs based on SMs:$PC_{71}BM$ active layers with different blend composition ratios.

Photoactive layer	Weight ratio	V_{oc} (V)	J_{sc} (mA cm^{-2})	FF (%)	PCE (%)
$BDT(TTzT)_2$:$PC_{71}BM$	2:1	0.94	2.84	34.5	0.92
	1.5:1	0.99	2.81	43.8	1.22
	1:1	0.96	2.74	37.9	1.00
	1:1.5	0.97	2.23	33.7	0.73
$BDT(TTz2T)_2$:$PC_{71}BM$	2:1	0.84	2.25	29.6	0.56
	1.5:1	0.91	1.79	38.7	0.63
	1:1	0.92	3.10	41.7	1.19
	1:1.5	0.88	2.68	41.5	0.98

bandgap of these SMs were calculated according to following equations [37,38]:

$$\mathrm{HOMO(eV)} = -\mathrm{e}(E_{ox}^{onset} + 4.54)$$

$$\mathrm{LUMO(eV)} = -\mathrm{e}(E_{\mathrm{red}}^{\mathrm{onset}} + 4.54)$$

$$E_g^{ec}(\mathrm{eV}) = e(E_{ox}^{onset} - E_{red}^{onset})$$

where E_{ox}^{onset} and E_{red}^{onset} are the measured onset potentials relative to Ag/Ag^+.

The results of the electrochemical measurements and the calculated energy levels of the synthesized molecules are summarized in Table 1. The calculated HOMO and LUMO energy levels of $BDT(TTzT)_2$ are −5.51 and −3.67 eV, respectively. The LUMO energy level of $BDT(TTz2T)_2$ is −3.64 eV which is similar to that of $BDT(TTzT)_2$. It indicates that the π-bridge length and end units in molecule backbone have almost no effect on the LUMO energy level of these molecules. For $BDT(TTz2T)_2$, the HOMO energy level shift upward by 0.21 eV compared with HOMO of $BDT(TTzT)_2$, which results in the decrease of the band gap and thus the broader light absorption. In addition, we also noticed that the HOMO energy levels of −5.51 eV for $BDT(TTzT)_2$ and −5.30 eV for BDT $(TTz2T)_2$ are still deeper than most other polythiophene derivative [39,40]. The deep HOMO energy levels of the two new molecules can help to improve the V_{oc}s when fabricating the photovoltaic devices with one of these SMs as donor and PCBM as the acceptor. The electrochemical band gaps of the molecules were calculated to be 1.84 and 1.66 eV, which is slightly smaller than their optical bandgap.

To better understand the oxidative and reductive properties of $BDT(TTzT)_2$ and $BDT(TTz2T)_2$, the electronic properties of these two molecules were calculated by density functional theory (DFT) at the DFT B3LYP/6-31G* level. Fig. 4 shows the geometry and the HOMO and LUMO wave functions. To simplify the calculation, all of the alkyl chains of these molecules were replaced by CH_3 groups. The electron density of LUMO levels for synthesized molecules mainly delocalizes on the Tz acceptor unit and the adjacent thiophene ring. Thus, the change of π-bridge length and end units has almost no effect on the LUMO levels. However, the electron density for HOMO is distributed over the whole molecule backbone, which indicates the donor unit, acceptor unit and π-bridge length significantly affect the HOMO level of these molecules. Meanwhile, The HOMO and LUMO level variation laws from the calculation are in agreement with the experimental results estimated from the electrochemical test.

2.4. Photovoltaic properties

In order to investigate the effect of π-bridge length and end units in SMs on the photovoltaic properties, and further demonstrate the potential application of the $BDT(TTzT)_2$ and $BDT(TTz2T)_2$ in OSCs, regular devices with a conventional structure of ITO/PEDOT:PSS(40 nm)/SM:$PC_{71}BM$/LiF(0.6 nm)/Al(100 nm) were fabricated. Detailed processes for device fabrication were described in Section 4. The weight ratio of both SMs:$PC_{71}BM$ was optimized from 2:1, 1.5:1, 1:1 and 1:1.5 and the relative photovoltaic parameters under one sun (simulated AM 1.5 G irradiation with intensity of 100 mW cm^{-2}) are summarized in Table 2. Using chlorobenzene (CB) as solvent, the SMs:$PC_{71}BM$ based devices afford high V_{oc}s up to 0.99 V and 0.92 V for $BDT(TTzT)_2$ and BDT $(TTz2T)_2$ respectively, resulting from the deep HOMO energy levels of these molecules. However, their efficiencies are compromised by very low short-circuit currents (J_{sc}s) and fill factors (FF).

The high absorption coefficient and relatively broad absorption range of these two molecules encouraged us to find out the reason for the low J_{sc}s by investigating the morphology of blend films. So we measured the surface morphology of these SMs:$PC_{71}BM$ blend films with different weight ratio by using Atomic force microscopy (AFM), as shown in Fig. 5. It clearly revealed that no matter what kind of weight ratio, the films fabricated from CB show strong aggregations with large isolated domains size of several hundred nanometers. These large isolated domains are not favorable for efficient excitons dissociation at the SM/$PC_{71}BM$ interfaces and charge transport in the active layer. This might be one of the main reasons for the low J_{sc}s. It is worthwhile to note that the processing additive, 1,8-diiodooctane (DIO), played an important role in improving the nanoscale morphology of the active layer [41–43]. So, we incorporated 0.5% v/v DIO into the blend solution of 1.5:1 for $BDT(TTzT)_2$:$PC_{71}BM$ and 1:1 for $BDT(TTz2T)_2$:$PC_{71}BM$. Interestingly, the performance of solar cells based on these two SMs was remarkably enhanced. Fig. 6 presented the current density-voltage (*J-V*) characteristics of devices. The corresponding V_{oc}, J_{sc}, FF, PCE as well as series resistance (R_s) and shunt resistance (R_{sh}) derived from Fig. 6 are listed in Table 3. Upon incorporation of DIO, the $BDT(TTzT)_2$ based device exhibits a PCE of 5.01% with a J_{sc} of 9.56 mA cm^{-2}, a V_{oc} of 0.98 V and a FF of 54%. In contrast, the BDT $(TTz2T)_2$ based device exhibits a higher PCE of 5.29% with an enhanced J_{sc} of 10.55 mA cm^{-2}, a V_{oc} of 0.88 V and a FF of 57%. Compared to the only-CB devices, the photovoltaic parameters that changed significantly are J_{sc} and FF, while the V_{oc} only slightly decrease. Meanwhile, the increased R_{sh} and decreased R_s indicate that the diode quality is improved when DIO was utilized as the solvent additive for both $BDT(TTzT)_2$ and $BDT(TTz2T)_2$ material systems. These improvements were consistent with underlying morphology changes as presented in Fig. 5 (images b1 and g1). When DIO was added into the CB solution, the blend film exhibited much more uniform and relatively smooth surface, where the big domains were broken into pieces, indicating a better miscibility and larger interface in active layers. As a result, the device performances were greatly increased. On the other hand,

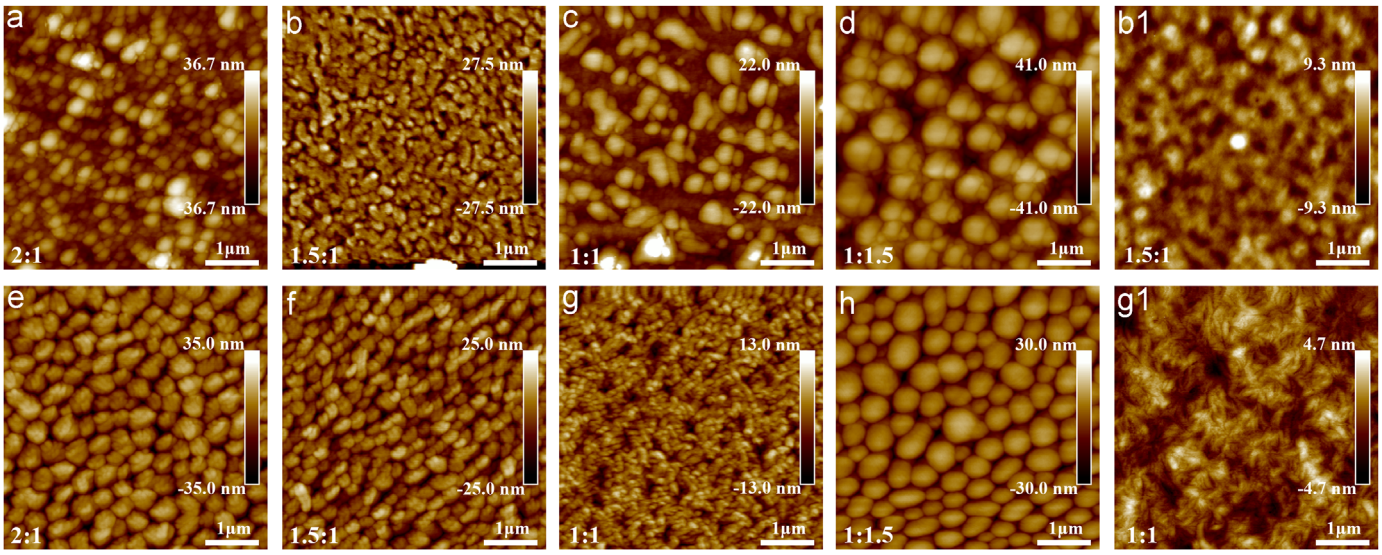

Fig. 5. AFM topographic images of the active layers with (a) BDT(TTzT)$_2$:PC$_{71}$BM (2:1, w/w), (b) BDT(TTzT)$_2$:PC$_{71}$BM (1.5:1, w/w), (c) BDT(TTzT)$_2$:PC$_{71}$BM (1:1, w/w), (d) BDT(TTzT)$_2$:PC$_{71}$BM (1:1.5, w/w), (b1) BDT(TTzT)$_2$:PC$_{71}$BM (1.5:1, w/w) with addition of 0.5% v/v DIO, (e) BDT(TTz2T)$_2$:PC$_{71}$BM (2:1, w/w), (f) BDT(TTz2T)$_2$:PC$_{71}$BM (1.5:1, w/w), (g) BDT(TTz2T)$_2$:PC$_{71}$BM (1:1, w/w), (h) BDT(TTz2T)$_2$:PC$_{71}$BM (1:1.5, w/w), (g1) BDT(TTz2T)$_2$:PC$_{71}$BM (1:1, w/w) with addition of 0.5% v/v DIO.

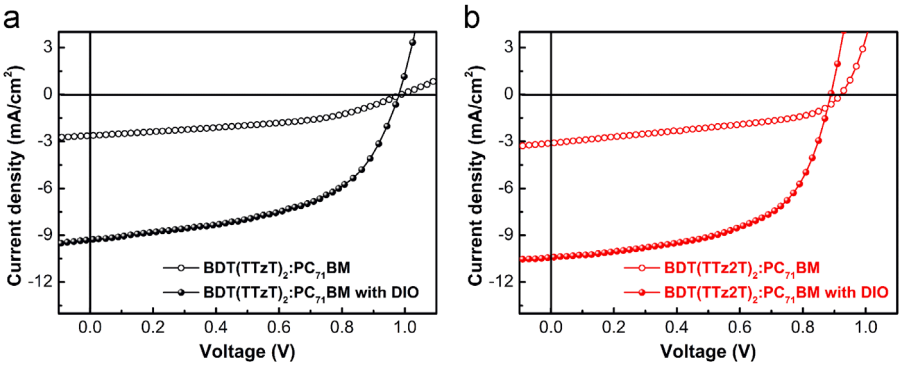

Fig. 6. J–V curves of the solar cells with an active layer composed of BDT(TTzT)$_2$:PC$_{71}$BM (1.5:1, w/w) and BDT(TTz2T)$_2$:PC$_{71}$BM (1:1, w/w) under the illumination of AM 1.5 G, 100 mW cm^2.

Table 3
Summary of device parameters of OSCs based on SMs:PC$_{71}$BM active layers with or without addition of DIO (0.5% v/v).

Photoactive layer	V_{oc} (V)	J_{sc} (mA cm^{-2})	FF (%)	PCE (%)	R_s (Ω cm^2)	R_{sh} (Ω cm^2)
BDT(TTzT)$_2$:PC$_{71}$BM	0.99	2.81	43.8	1.22	46.1	608.1
BDT(TTz2T)$_2$: PC$_{71}$BM	0.92	3.10	41.7	1.19	31.4	530.9
BDT(TTzT)$_2$:PC$_{71}$BM with DIO	0.98	9.56	53.5	5.01	12.1	866.7
BDT(2TTzT)$_2$: PC$_{71}$BM with DIO	0.88	10.55	57.2	5.29	10.7	937.6

comparing these two optimized SM solar cells, although the V_{oc} of BDT(TTz2T)$_2$ based device is lower than that of BDT(TTzT)$_2$, the efficiency was compensated by its higher J_{sc} and FF, which should stem from the strong intermolecular interaction, the broader absorption and larger absorption coefficient induced by extending conjugated length in the BDT(TTz2T)$_2$ backbone. Besides, from Fig. 5 (image g1) it can be seen that the BDT(TTz2T)$_2$:PC$_{71}$BM film shows a finely intermixed phase separation with fibrous features emerged, explaining the relatively higher FF of BDT(TTz2T)$_2$ based device.

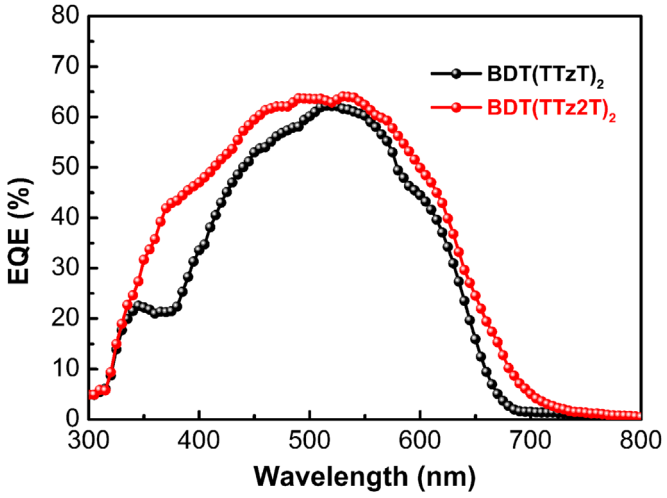

Fig. 7. The EQE of OSCs based on BDT(TTzT)$_2$:PC$_{71}$BM (1.5:1, w/w) and BDT(TTz2T)$_2$:PC$_{71}$BM (1:1, w/w) with DIO (0.5% v/v).

We also measured the external quantum efficiency (EQE) of the devices to evaluate the spectral dependence of the photocurrent, as shown in Fig. 7. Apparently, the BDT(TTz2T)$_2$ based device shows a broader response range (300–700 nm) and more efficient

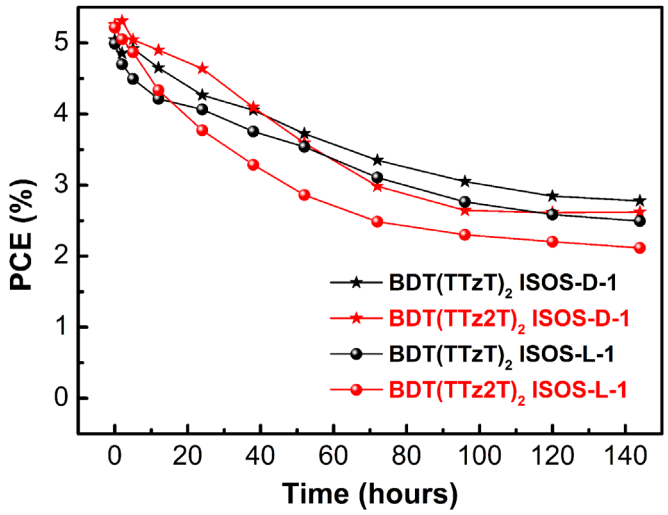

Fig. 8. The PCE characteristics curve as a function of storage time for OSCs based on $BDT(TTzT)_2$:$PC_{71}BM$ and $BDT(TTz2T)_2$:$PC_{71}BM$.

incident-photon to current conversion than $BDT(TTzT)_2$ based device, with peak EQE values at 64% for $BDT(TTz2T)_2$ and 62% for $BDT(TTzT)_2$. The different EQE response could be ascribed to the different absorption characteristics of these two SMs. The calculated J_{sc}s from EQE curves by using a standard AM 1.5G spectrum match well with those obtained from *J-V* measurement.

The stability test of the devices was also performed according to ISOS-D-1 (dark storage) and ISOS-L-1 (light soaking) standards [44,45]. Fig. 8 shows the degradation of PCEs along with the storage time. For ISOS-D-1 test, PCEs remain 55% and 50% of initial values after 144 h for devices based on $BDT(TTzT)_2$ and $BDT(TTz2T)_2$ respectively. Under ISOS-L-1 condition, the devices exhibited similar degradation tendency with ISOS-D-1 test. Especially for the $BDT(TTzT)_2$ based device, it can still retain about 50% of initial value until the end of test. Compared with $BDT(TTzT)_2$ based devices, the $BDT(TTz2T)_2$ based devices showed slightly rapid degradation under ISOS-L-1 condition, which is likely due to the higher HOMO levels of $BDT(TTz2T)_2$. It should be note that these results are obtained from un-encapsulated devices, we believe that better stability can be achieved by rational encapsulation.

3. Conclusion

In conclusion, we have designed and synthesized two new SMs, $BDT(TTzT)_2$ and $BDT(TTz2T)_2$ with D2-A-D1-A-D2 structure, where BDT as the central building block and electron donating unit and Tz as an electron acceptor unit. They exhibited relatively broad optical absorption spectra, high molar absorption coefficient and good solubility in common organic solvents. The introduction of Tz acceptor unit lowers both HOMO and LUMO energy levels of synthesized molecules. As expected, two molecules showed low-lying HOMO energy levels (-5.51 and -5.30 eV) assured a relatively large V_{oc} when they were used in photovoltaic devices. V_{oc} of 0.98 and 0.88 eV were obtained by $BDT(TTzT)_2$ and $BDT(TTz2T)_2$ based OSCs, with promising PCE of 5.01% and 5.29%, respectively.

4. Experimental section

4.1. Measurements and characterization

^{1}H NMR and ^{13}C NMR spectra were recorded on Varian Mercury 300 MHz spectrometer and Bruker AVANCE 500 MHz spectrometer with chloroform-d as solvent and tetramethylsilane (TMS) as internal standard. The optical absorption spectra of the organic molecules were measured by a Shimadzu UV–1700 spectrophotometer. Electrochemical measurement of these molecules was performed with a Bioanalytical Systems BAS 10 B/W electrochemical workstation.

4.2. Fabrication and characterization of photovoltaic cells

SMs solar cells were fabricated with device structure of ITO/PEDOT:PSS/SM:$PC_{71}BM$/LiF/Al. Prior to fabrication, the patterned ITO glass substrates (15 Ω/square) were cleaned by sequential ultrasonic treatment in detergent, deionized water, acetone and isopropyl alcohol. Then the substrates were dried by nitrogen flow and exposed to UV-Ozone treatment for 10 min, The PEDOT:PSS (Clevios P VP AI 4083) aqueous dispersion were spin-coated (5000 rpm for 50 s) onto the ITO substrates at a thickness of ~40 nm (after passing through a 0.22 μm filter). Then the substrates were annealed at 140 °C for 30 min in air and transferred into a glove box. Blend solutions for the active layers were prepared by dissolving SMs and $PC_{71}BM$ with different weight ratio (from 2:1, 1.5:1, 1:1 and 1:1.5). The processing solvent is chlorobenzene or chlorobenzene/1,8-diiodooctane mixed solvent with a SMs concentration of 8 mg/mL for $BDT(TTzT)_2$ and 10 mg/mL for $BDT(TTz2T)_2$. The blend solution was stirred in a glove box for at least 24 h before film casting. The BHJ active layers can be obtained by spin-coating the aforementioned solutions at 1000 rpm for 50 s on top of the PEDOT:PSS film (after passing through a 0.45 μm filter) in argon-filled glove box. The devices were finally completed by thermal evaporation of a 0.6 nm thick LiF and a 100 nm thick aluminum cathode in vacuum (vacuum degree $\approx 5 \times 10^{-4}$ Pa) with a shadow mask (device active area of about 0.064 cm^2). The current density-voltage (*J-V*) characteristics of fabricated devices were measured using Keithley 2400 Source Meter in dark and under Air Mass 1.5 Global (AM 1.5 G) solar illuminations with an Oriel 300 W solar simulator intensity of 100 mW/cm^2. The light intensity was measured by a photometer (International light, IL1400) and corrected by a standard silicon solar cell. The surface morphologies and external quantum efficiency (EQE) spectra were measured using atomic force microscopy (AFM, Veeco Dimension 3100) and Crowntech QTest Station 1000 CE, respectively. All the measurements were performed under ambient atmosphere at room temperature.

4.3. Materials

All starting materials were purchased from either Acros or Aldrich Chemical Co. and used without further purification, unless otherwise noted. In synthetic preparations, diethyl ether, tetrahydrofuran (THF) and toluene were dried by distillation from sodium/benzophenone under nitrogen. Similarly, *N*,*N*-Dimethylformamide (DMF) and dichloromethane were distilled from CaH_2 under nitrogen. Compound 1 [27], compound 3 [31] trimethyl(5-hexylthiophen-2-yl) stannane [34] and tributyl(4-hexylthiophen-2-yl)stannane [46], were synthesized according to literature procedures.

4.4. Synthesis

4.4.1. 3-(5-bromo-4-hexyl-2-thienyl)-6-(3,5′-dihexyl-2,2′-bithiophen-5-yl)-1,2,4,5-tetrazine (2)

Trimethyl(5-hexylthiophen-2-yl)stannane (0.58 g, 1.75 mmol) and 3,6-Bis(5-bromo-4-hexyl-2-thienyl)-1,2,4,5-tetrazine (1) (1.0 g, 1.75 mmol) were placed in a round-bottom flask (50 mL) with $Pd(PPh_3)_4$ (40 mg) and then the flask was evacuated and back-filled with nitrogen three times followed by 15 mL of anhydrous toluene added through a syringe. The mixture was stirred

under nitrogen at 90 °C for 18 h. The reaction mixture was poured into water before extracted with chloroform and the collected organic phase was dried over anhydrous $MgSO_4$. After removing the solvent by rotary evaporator, the product was purified by silica gel chromatography using a mixture of petroleum ether and chloroform (4:1) as eluant to yield product as red solid (542 mg, 47%).

^{1}H NMR (300 MHz, $CDCl_3$, TMS): δ (ppm) 8.04 (s, 1H), 7.91 (s, 1H), 7.11 (d, J=3.6 Hz, 1H), 6.78 (d, J=3.6 Hz, 1H), 2.90–2.77 (m, 4H), 2.63 (t, J=7.2 Hz, 2H), 1.77–1.62 (m, 6H), 1.65–1.27 (m, 18H), 0.86–0.95 (m, 9H).

4.4.2. BDT(TTzT)$_2$

Compound 2 (433 mg, 0.656 mmol) and 2,6-bis(trimethyltin)-4.8-bis(2-ethylhexyloxy)benzo[1,2-b:4,5-b′]dithiophene (3) (230 mg, 0.298 mmol) were placed in a round-bottom flask (50 mL) with Pd$(PPh_3)_4$ (20 mg) and then the flask was evacuated and back-filled with nitrogen three times followed by 3 mL of DMF and 15 mL of anhydrous toluene added through a syringe. The mixture was stirred under nitrogen at 90 °C for 25 h. The reaction mixture was poured into water before extracted with chloroform and the collected organic phase was dried over anhydrous $MgSO_4$. After removing the solvent by rotary evaporator, the product was purified by silica gel chromatography using a mixture of petroleum ether and chloroform (3:1) as eluant to yield product as dark red solid (206 mg, 43%).

^{1}H NMR (300 MHz, $CDCl_3$, TMS): δ (ppm) 8.07 (d, J=6.9 Hz, 4H), 7.59 (s, 2H), 7.11 (d, J=3.6 Hz, 2H), 6.78 (d, J=3.6 Hz, 2H), 4.25 (d, J=5.1 Hz, 4H), 2.97 (t, J=7.8 Hz, 4H), 2.90–2.75 (m, 8H), 1.84–1.62 (m, 18H), 1.53–1.23 (m, 48H), 1.08 (t, J=7.2 Hz, 6H), 1.03–0.82 (m, 24H). ^{13}C NMR (125 MHz, $CDCl_3$) δ 160.72, 160.43, 147.69, 144.09, 142.02, 140.26, 139.17, 138.09, 135.27, 133.71, 133.41, 133.23, 132.81, 132.17, 131.96, 129.52, 126.57, 124.65, 119.04, 76.01, 40.77, 31.95, 31.83, 31.70, 31.59, 31.47, 31.38, 30.57, 30.23, 30.18, 29.72, 29.55, 29.38, 29.32, 28.91, 23.95, 23.24, 22.75, 22.67, 22.62, 14.28, 14.12, 14.10, 14.08, 11.46.

4.4.3. 3,6-Bis(3,4′-dihexyl-2,2′-bithiophen-5-yl)-1,2,4,5-tetrazine (4)

Tributyl(4-hexylthiophen-2-yl)stannane (2.08 g, 4.54 mmol) and compound 1 (1.0 g, 1.75 mmol) were placed in a round-bottom flask (50 mL) with Pd$(PPh_3)_2Cl_2$ (61 mg) and then the flask was evacuated and back-filled with nitrogen three times followed by 15 mL of anhydrous toluene added through a syringe. The mixture was stirred under nitrogen at 90 °C for 18 h. The reaction mixture was poured into water before extracted with chloroform and the collected organic phase was dried over anhydrous $MgSO_4$. After removing the solvent by rotary evaporator, the product was purified by silica gel chromatography using a mixture of petroleum ether and chloroform (3:1) as eluant to yield product as red solid (1.12 g, 86%).

^{1}H NMR (300 MHz, $CDCl_3$, TMS): δ (ppm) 8.07 (s, 2H), 7.13 (d, J=1.2 Hz, 2H), 7.00 (d, J=1.5 Hz, 2H), 2.84 (t, J=7.8 Hz, 4H), 2.64 (t, J=7.8 Hz, 4H), 1.79–1.60 (m, 8H), 1.44–1.28 (m, 24H), 0.94–0.84 (m, 12H).

4.4.4. 3,6-Bis(5′-bromo-3,4′-dihexyl-2,2′-bithiophen-5-yl)-1,2,4,5-tetrazine (5)

A round-bottom flask which placed in compound 4 (891 mg, 1.19 mmol) and *N*-bromosuccinimide (NBS) (466 mg, 2.62 mmol) was evacuated and back-filled with nitrogen three times followed by 27 mL of chloroform and 27 mL of ethanoic acid added through syringes. The mixture was stirred under nitrogen at room temperature for 1 h in dark then heat to refluxed and stirred for 8 h. The mixture was washed with solution of $NaHCO_3$ in water three times, and dried over anhydrous $MgSO_4$. After removing the solvent by rotary evaporator, the product was purified by silica gel chromatography using a mixture of petroleum ether and chloroform (7:1) as eluant to yield product as red solid (947 mg, 88%).

^{1}H NMR (300 MHz, $CDCl_3$, TMS): δ (ppm) 8.06 (s, 2H), 6.98 (s, 2H), 2.80 (t, J=7.5 Hz, 4H), 2.60 (t, J=7.2 Hz, 4H), 1.77–1.59 (m, 8H), 1.45–1.29 (m, 24H), 0.95–0.83 (m, 12H).

4.4.5. 3-(5′-bromo-3,4′-dihexyl-2,2′-bithiophen-5-yl)-6-(3,4′,5′-trihexyl-2,2′-5′2′-terthiophene-5yl)-1,2,4,5-tetrazine (6)

Trimethyl(5-hexylthiophen-2-yl)stannane (274 mg, 0.83 mmol) and compound 5 (750 mg, 0.83 mmol) were placed in a round-bottom flask (50 mL) with Pd$(PPh_3)_4$ (19 mg) and then the flask was evacuated and back-filled with nitrogen three times followed by 15 mL of dried toluene added through a syringe. The mixture was stirred under nitrogen at 90 °C for 15 h. The reaction mixture was poured into water before extracted with chloroform and the organic layer was dried over anhydrous $MgSO_4$. After removing the solvent by rotary evaporator, the product was purified by silica gel chromatography using a mixture of petroleum ether and chloroform (6:1) as eluant to yield product as red solid (370 mg, 45%).

^{1}H NMR (300 MHz, $CDCl_3$, TMS): δ (ppm) 8.06 (d, J=4.8 Hz, 2H), 7.13 (s, 1H), 6.98 (t, J=1.2 Hz, 2H), 6.76 (d, J=3.6 Hz, 1H), 2.91–2.72 (m, 8H), 2.59 (t, J=7.5 Hz, 2H), 1.78–1.60 (m, 10H), 1.45–1.28 (m, 30H), 0.90 (t, J=6.9 Hz, 15H).

4.4.6. BDT(TTz2T)$_2$

Compound 6 (317 mg, 0.48 mmol) and 2,6-bis(trimethyltin)-4.8-bis(2-ethylhexyloxy)benzo[1,2-b:4,5-b′]dithiophene (3) (169 mg, 0.22 mmol) were placed in a round-bottom flask (50 mL) with Pd$(PPh_3)_4$ (20 mg) and then the flask was evacuated and back-filled with nitrogen three times followed by 10 mL of dried toluene and 3 mL of dried DMF added through syringes. The mixture was stirred under nitrogen at 90 °C for 28 h. The reaction mixture was poured into water before extracted with chloroform and the collected organic phase was dried over anhydrous $MgSO_4$. After removing the solvent by rotary evaporator, the product was purified by silica gel chromatography using a mixture of petroleum ether and chloroform (2.5:1) as eluant to yield product as dark red solid (188 mg, 38%).

^{1}H NMR (500 MHz, $CDCl_3$, TMS): δ (ppm) 7.97 (d, J=2.0 Hz, 4H), 7.38 (s, 2H), 7.09 (s, 2H), 7.06 (s, 2H), 6.94 (d, J=3.5 Hz, 2H), 6.71 (d, J=3.5 Hz, 2H), 4.24–4.14 (m, 4H), 2.97–2.77 (m, 16H), 2.74 (t, J=8.0 Hz, 4H), 1.90–1.62 (m, 26H), 1.52–1.97 (m, 72H), 1.12 (t, J=7.5 Hz, 6H), 1.04–0.89 (m, 36H). ^{13}C NMR (125 MHz, $CDCl_3$) δ 160.44, 146.45, 140.48, 139.11, 138.32, 133.23, 132.94, 132.70, 132.49, 132.32, 129.32, 125.53, 124.36, 117.38, 75.62, 40.71, 31.90, 31.83, 31.73, 31.61, 31.51, 30.57, 30.49, 30.16, 30.12, 29.72, 29.68, 29.49, 29.36, 28.92, 23.91, 23.23, 22.82, 22.75, 22.71, 22.63, 14.31, 14.19, 14.18, 14.14, 14.10, 11.46.

Acknowledgements

This work was supported by the National Natural Science Foundation of China (Grant Nos. 51303061, 11574110), the Project of Science and Technology Development Plan of Jilin Province (Grant No. 20140204056GX), the Project of Science and Technology Plan of Changchun City (Grant No. 13KG49), Opened Fund of the State Key Laboratory on Applied Optics, and the China Postdoctoral Science Foundation (Grant Nos. 2014T70288, 2013M541299).

References

[1] G. Yu, J. Gao, J.C. Hummelen, F. Wudl, A.J. Heeger, Polymer photovoltaic cells: enhanced efficiencies via a network of internal donor-acceptor heterojunctions, Science 270 (1995) 1789–1791.

[2] E. Bungaard, F.C. Krebs, Low band gap polymers for organic photovoltaics, Sol. Energy Mater. Sol. Cells 91 (2007) 954–985.

[3] F.C. Krebs, Fabrication and processing of polymer solar cells: a review of printing and coating techniques, Sol. Energy Mater. Sol. Cells 93 (2009) 394–412.

[4] Y.H. Zhou, C. Fuentes-Hernandez, J. Shim, J. Meyer, A.J. Giordano, H. Li, P. Winget, T. Papadopoulos, H. Cheun, J. Kim, M. Fenoll, A. Dindar, W. Haske, E. Najafabadi, T.M. Khan, H. Sojoudi, S. Barlow, S. Graham, J.-L. Brédas, S. R. Marder, A. Kahn, B. Kippelen, A universal method to produce low-work function electrodes for organic electronics, Science 336 (2012) 327–332.

[5] M. Helgesen, J.E. Carlé, G.A. dos Reis Benatto, R.R. Søndergaard, M. Jørgensen, E. Bundgaard, F.C. Krebs, Making ends meet: flow synthesis as the answer to reproducible high-performance conjugated polymers on the scale that roll-to-roll processing demands, Adv. Energy Mater. 5 (2015) 1401996.

[6] F.C. Krebs, N. Espinosa, M. Hösel, R.R. Søndergaard, M. Jørgensen, 25th anniversary article: rise to power – OPV-based solar parks, Adv. Mater. 26 (2014) 29–39.

[7] M. Helgesen, R. Søndergaard, F.C. Krebs, Advanced materials and processes for polymer solar cell devices, J. Mater. Chem. 20 (2010) 36–60.

[8] Y.H. Zhou, C. Fuentes-Hernandez, J.W. Shim, T.M. Khan, B. Kippelen, High performance polymeric charge recombination layer for organic tandem solar cells, Energy Environ. Sci. 5 (2012) 9827–9832.

[9] V. Vohra, K. Kawashima, T. Kakara, T. Koganezawa, I. Osaka, K. Takimiya, H. Murata, Efficient inverted polymer solar cells employing favourable molecular orientation, Nat. Photonics 9 (2015) 403.

[10] Y.H. Liu, J.B. Zhao, Z.K. Li, C. Mu, W. Ma, H.W. Hu, K. Jiang, H.R. Lin, H. Ade, H. Yan, Aggregation and morphology control enables multiple cases of high-efficiency polymer solar cells, Nat. Commun. 5 (2014) 5293.

[11] J.D. Chen, C.H. Cui, Y.Q. Li, L. Zhou, Q.D. Ou, C. Li, Y.F. Li, J.X. Tang, Single-junction polymer solar cells exceeding 10% power conversion efficiency, Adv. Mater. 27 (2015) 1035–1041.

[12] B. Walker, C. Kim, T.-Q. Nguyen, Small molecule solution-processed bulk heterojunction solar cells, Chem. Mater. 23 (2011) 470–482.

[13] A.K.K. Kyaw, D.H. Wang, D. Wynands, J. Zhang, T.-Q. Nguyen, G.C. Bazan, A. J. Heeger, Improved light harvesting and improved efficiency by insertion of an optical spacer (ZnO) in solution-processed small-molecule solar cells, Nano Lett. 13 (2013) 3796–3801.

[14] T. Harschneck, N. Zhou, E.F. Manley, S.J. Lou, X. Yu, M.R. Butler, A. Timalsina, R. Turrisi, M.A. Ratner, L.X. Chen, R.P.H. Chang, A. Facchetti, T.J. Marks, Substantial photovoltaic response and morphology tuning in benzo[1,2-b:6,5-b′] dithiophene (bBDT) molecular donors, Chem. Commun. 50 (2014) 4099–4101.

[15] H.T. Bai, Y.F. Wang, P. Cheng, Y.F. Li, D.B. Zhu, X.W. Zhan, Acceptor-donor-acceptor small molecules based on indacenodithiophene for efficient organic solar cells, ACS Appl. Mater. Interfaces 6 (2014) 8426–8433.

[16] Y.S. Liu, C.C. Chen, Z.R. Hong, J. Gao, Y.M. Yang, H.P. Zhou, L.T. Dou, G. Li, Y. Yang, Solution-processed small-molecule solar cells: breaking the 10% power conversion efficiency, Sci. Rep. 3 (2013) 3356.

[17] V. Gupta, A.K.K. Kyaw, D.H. Wang, S. Chand, G.C. Bazan, A.J. Heeger, Barium: an efficient cathode layer for bulk-heterojunction solar cells, Sci. Rep. 3 (2013) 1965.

[18] B. Kan, M.M. Li, Q. Zhang, F. Liu, X.J. Wan, Y.C. Wang, W. Ni, G.K. Long, X. Yang, H.R. Feng, Y. Zuo, M.T. Zhang, F. Huang, Y. Cao, T.P. Russell, Y.S. Chen, A series of simple oligomer-like small molecules based on oligothiophenes for solution-processed solar cells with high efficiency, J. Am. Chem. Soc. 137 (2015) 3886–3893.

[19] Q. Zhang, B. Kan, F. Liu, G.K. Long, X.J. Wan, X.Q. Chen, Y. Zuo, W. Ni, H.J. Zhang, M.M. Li, Z.C. Hu, F. Huang, Y. Cao, Z.Q. Liang, M.T. Zhang, T.P. Russell, Y.S. Chen, Small-molecule solar cells with efficiency over 9%, Nat. Photonics 9 (2014) 35–41.

[20] S.P. Wen, C. Wang, P.F. Ma, Y.-X. Zhao, C. Li, S.P. Ruan, Synthesis and photovoltaic properties of dithieno[3,2-b:2′,3′-d]silole-based conjugated copolymers, J. Mater. Chem. A 3 (2015) 13794–13800.

[21] C. Zhang, H. Li, J.Z. Wang, Y.F. Zhang, Y. Qiao, D.Z. Huang, C.-A. Di, X.W. Zhan, X. Z. Zhu, D.B. Zhu, Low-bandgap thieno[3,4-c]pyrrole-4,6-dione-polymers for high-performance solar cells with significantly enhanced photocurrents, J. Mater. Chem. A 3 (2015) 11194–11198.

[22] S.P. Wen, C. Wang, P.F. Ma, G. Wang, W. Dong, Y.J. Gao, S.P. Ruan, Improved efficiency in dithieno[3,2-b:2′,3′-d]silole-based polymer solar cells by the insertion of ZnO optical spacer, J. Phys. Chem. C 119 (2015) 20817–20822.

[23] M.C. Scharber, D. Mühlbacher, M. Koppe, P. Denk, C. Waldauf, A.J. Heeger, C. J. Brabec, Design rules for donors in bulk-heterojunction solar cells—towards 10% energy-conversion efficiency, Adv. Mater. 18 (2006) 789–794.

[24] S.P. Wen, J.N. Pei, Y.H. Zhou, L.L. Xue, B. Xu, Y.W. Li, W.J. Tian, Synthesis and photovoltaic properties of poly(*p*-phenylenevinylene) Derivatives containing oxadiazole, J. Polym. Sci. Part A: Polym. Chem. 47 (2009) 1003–1012.

[25] Y.W. Li, L.L. Xue, H. Li, Z.F. Li, B. Xu, S.P. Wen, W.J. Tian, Energy level and molecular structure engineering of conjugated donor–acceptor copolymers for photovoltaic applications, Macromolecules 42 (2009) 4491–4499.

[26] W.D. Cheng, Z.H. Wu, S.P. Wen, B. Xu, H. Li, F.R. Zhu, W.J. Tian, Donor–acceptor copolymers incorporating polybenzo[1,2-b:4,5-b′]dithiophene and tetrazine for high open circuit voltage polymer solar cells, Org. Electron. 14 (2013) 2124–2131.

[27] Z. Li, J.F. Ding, N.H. Song, J.P. Lu, Y. Tao, Development of a new s-tetrazine-based copolymer for efficient solar cells, J. Am. Chem. Soc. 132 (2010) 13160–13161.

[28] Z. Li, J.F. Ding, N.H. Song, X.M. Du, J.Y. Zhou, J.P. Lu, Y. Tao, Alternating copolymers of dithienyl-s-tetrazine and cyclopentadithiophene for organic photovoltaic applications, Chem. Mater. 23 (2011) 1977–1984.

[29] S.P. Wen, Q.F. Dong, W.D. Cheng, P.F. Li, B. Xu, W.J. Tian, A benzo[1,2-b:4,5-b′] dithiophene-based copolymer with deep HOMO level for efficient polymer solar cells, Sol. Energy Mater. Sol. Cells 100 (2012) 239–245.

[30] Y.J. Chen, C. Li, P. Zhang, Y.W. Li, X.M. Yang, L.W. Chen, Y.F. Tu, Solution-processable tetrazine and oligothiophene based linear A–D–A small molecules: synthesis, hierarchical structure and photovoltaic properties, Org. Electron. 14 (2013) 1424–1434.

[31] J.H. Hou, M.-H. Park, S.Q. Zhang, Y. Yao, L.-M. Chen, J.-H. Li, Y. Yang, Bandgap and molecular energy level control. of conjugated polymer photovoltaic materials based on benzo[1,2-b:4,5-b′]dithiophene, Macromolecules 41 (2008) 6012–6018.

[32] Y.S. Liu, X.J. Wan, F. Wang, J.Y. Zhou, G.K. Long, J.G. Tian, Y.S. Chen, High-performance solar cells using a solution-processed small molecule containing benzodithiophene unit, Adv. Mater. 23 (2011) 5387–5391.

[33] J.Y. Zhou, X.J. Wan, Y.S. Liu, Y. Zuo, Z. Li, G.R. He, G.K. Long, W. Ni, C.X. Li, X. C. Su, Y.S. Chen, Small molecules based on benzo[1,2-b:4,5-b′]dithiophene unit for high-performance solution-processed organic solar cells, J. Am. Chem. Soc. 134 (2012) 16345–16351.

[34] C.-Y. Yu, B.-T. Ko, C. Ting, C.-P. Chen, Two-dimensional regioregular polythiophenes with conjugated side chains for use in organic solar cells, Sol. Energy Mater. Sol. Cells 93 (2009) 613–620.

[35] Z. Pan, Y. Liu, F. Fan, Y. Chen, Y.X. Li, X.W. Zhan, Y. Song, Self-assembled π-extended condensed benzothiophene nanoribbons for field-effect transistors, Chem. Eur. 19 (2013) 9771–9774.

[36] T. Yamamoto, D. Komarudin, M. Arai, B.-L. Lee, H. Suganuma, N. Asakawa, Y. Inoue, K. Kubota, S. Sasaki, T. Fukuda, H. Matsuda, Extensive studies on pi-stacking of poly(3-alkylthiophene-2,5-diyl)s and poly(4)-alkylthiazole-2,5-Diyl)s by optical spectroscopy, NMR analysis, light scattering analysis, and X-ray crystallography, J. Am. Chem. Soc. 120 (1998) 2047–2058.

[37] S.P. Wen, J.N. Pei, Y.H. Zhou, P.F. Li, L.L. Xue, Y.W. Li, B. Xu, W.J. Tian, Synthesis of 4,7-diphenyl-2,1,3-benzothiadiazole-based copolymers and their photovoltaic applications, Macromolecules 42 (2009) 4977–4984.

[38] S.P. Wen, W.D. Cheng, P.F. Li, S.Y. Yao, B. Xu, H. Li, Y.J. Gao, Z.L. Wang, W.J. Tian, Synthesis and Photovoltaic properties of thieno[3,4-c]pyrrole-4,6-dione-based Donor-Acceptor Copolymers, J. Polym. Sci. , Part A: Polym. Chem. 50 (2012) 3758–3766.

[39] C.J. Shi, Y. Yao, Y. Yang, Q.B. Pei, Regioregular copolymers of 3-alkoxythiophene and their photovoltaic application, J. Am. Chem. Soc. 128 (2006) 8980–8986.

[40] J. Cremer, P. Bäuerle, Star-shaped perylene–oligothiophene–triphenylamine hybrid systems for photovoltaic applications, J. Mater. Chem. 16 (2006) 874–884.

[41] Y.M. Sun, G.C. Welch, W.L. Leong, C.J. Takacs, G.C. Bazan, A.J. Heeger, Solution-processed small-molecule solar cells with 6.7% efficiency, Nat. Mater. 11 (2012) 44–48.

[42] E.-P. Yao, C.-C. Chen, J. Gao, Y.S. Liu, Q. Chen, M. Cai, W.-C. Hsu, Z.R. Hong, G. Li, Y. Yang, The study of solvent additive effects in efficient polymer photovoltaics via impedance spectroscopy, Sol. Energy Mater. Sol. Cells 130 (2014) 20–26.

[43] X. Cheng, Q. Wan, Y. Wu, B. Guo, X. Guo, Y.W. Li, M.J. Zhang, C.H. Cui, Y.F. Li, Toward high open-circuit voltage by smart chain engineering in 2D-conjugated polymer for polymer solar cells, Sol. Energy Mater. Sol. Cells 149 (2016) 162–169.

[44] M. Jørgensen, K. Norrman, S.A. Gevorgyan, T. Tromholt, B. Andreasen, F. C. Krebs, Stability of polymer solar cells, Adv. Mater. 24 (2012) 580–612.

[45] M.O. Reese, S.A. Gevorgyan, M. Jørgensen, E. Bundgaard, S.R. Kurtz, D.S. Ginley, D.C. Olson, M.T. Lloyd, P. Morvillo, E.A. Katz, A. Elschner, O. Haillant, T. R. Currier, V. Shrotriya, M. Hermenau, M. Riede, K.R. Kirov, G. Trimmel, T. Rath, O. Inganäs, F.L. Zhang, M. Andersson, K. Tvingstedt, M. Lira-Cantu, D. Laird, C. McGuiness, S. Gowrisanker, M. Pannone, M. Xiao, J. Hauch, R. Steim, D. M. DeLongchamp, R. Rösch, H. Hoppe, N. Espinosa, A. Urbina, G. Yaman-Uzunoglu, J.-B. Bonekamp, A.J.J.M. van Breemen, C. Girotto, E. Voroshazi, F. C. Krebs, Consensus stability testing protocols for organic photovoltaic materials and devices, Sol. Energy Mater. Sol. Cells 95 (2011) 1253–1267.

[46] S.P. Wen, J.N. Pei, P.F. Li, Y.H. Zhou, W.D. Cheng, Q.F. Dong, Z.F. Li, W.J. Tian, Synthesis and Photovoltaic properties of Low-Bandgap 4,7-dithien-2-yl-2,1,3-benzothiadiazole-based poly(heteroarylenevinylene)s, J. Polym. Sci. Part A: Polym. Chem. 49 (2011) 2715–2724.